Axial dispersion in segmented gas-liquid flow: Effects of alternating channel curvature

Metin Muradoglu[a)]
Department of Mechanical Engineering, Koc University, Rumelifeneri Yolu Sariyer, Istanbul 34450, Turkey

(Received 31 March 2010; accepted 6 December 2010; published online 30 December 2010)

The effects of channel curvature on the axial dispersion in segmented gas-liquid flows are studied computationally in a two-dimensional setting using a finite-volume/front-tracking method. Passive tracer particles are used to visualize and quantify the axial dispersion. The molecular diffusion is modeled by random walk of tracer particles. It is found that there is significant axial dispersion in serpentine channels even in the absence of molecular diffusion. The lubricating thin liquid layer that persists on the wall of a straight channel is periodically broken in the serpentine channel leading to enhanced axial dispersion. It is also found that the axial dispersion is always larger in the serpentine channel than that in the straight channel but the effects of channel curvature are more pronounced at high Peclet numbers, i.e., $\mathrm{Pe}>10^4$. A model is proposed based on the difference between the liquid film thicknesses on the inner and outer side of the bend in the limit as $\mathrm{Pe}\rightarrow\infty$. Good agreement is found between the computational results and the model when the liquid slug is well mixed by the chaotic advection. © *2010 American Institute of Physics*. [doi:10.1063/1.3531742]

I. INTRODUCTION

Segmented gas-liquid flow (also known as Taylor flow) has been studied extensively since the pioneering works of Taylor[1] and Bretherton[2] due to its significance in a number of engineering processes such as two-phase catalytic monolith reactors,[3–6] polymer blow molding, enhanced oil recovery,[7] continuous-flow analysis of biological or chemical samples,[8–10] and rapid mixing of solutes in microchannels.[11] The micromixer developed by Günther *et al.*[11] is based on the chaotic stirring within the liquid slugs moving through a gas-segmented serpentine channel and it has been shown to reduce the mixing lengths two- to threefold as compared to passive mixers with patterned side walls or three dimensional channel geometries. In addition to the enhanced mixing, the segmentation also reduces the axial dispersion significantly compared to the single phase flow and only dispersion occurs due to either convection through liquid film between the channel wall and bubble or diffusion through the gas-liquid interface. Note that the liquid region between two centroids of bubbles is referred as *slug* while the recirculating region in the liquid slug is referred as *bolus* in the present study.

The quality of mixing within the liquid slugs strongly depends on the segmentation and the channel curvature as recently discussed by Dogan *et al.*[12] In the case of a straight channel, there are two contour rotating symmetrical steady vortices within the liquid slug in the coordinate system moving with the bubbles. Thus there is no cross mixing in the straight channel in the absence of molecular diffusion.[12,13] This symmetry is broken in the case of a serpentine channel and mixing is enhanced by the channel curvature.[12,13] However, the channel curvature also increases the axial dispersion that is usually unwanted in many applications. It is known that a lubricating thin liquid layer persists on the channel walls when the channel is straight. However this lubricating liquid layer is periodically broken in the serpentine channel case leading to enhanced axial dispersion. Muradoglu and Stone[14] showed that the film thickness on the inner wall is thinner than that on the outer wall and this difference in film thicknesses increases with channel curvature. As the liquid slugs move through a serpentine channel, the film thickness alternates periodically due to change in the channel curvature and thus significant amount of liquid leaks through the outer layer even in the absence of the molecular diffusion. Although axial dispersion is still much reduced in the segmented gas-liquid flow compared to the corresponding single phase flow, there may be significant backmixing especially in the case of large channel curvatures. This backmixing enlarges the residence time distribution and thus deteriorates performance of microreactors.[15–18] It is therefore of fundamental importance to understand and control the axial dispersion in gas-segmented serpentine channels.

The early studies on the gas-segmented flow were mainly motivated by the continuous-flow analyzers.[8] Recently, the gas-segmented flows have been mainly studied due to applications in monolith reactors[6,19–21] and enhanced mixing in microchannels.[11,15] Pedersen and Horvath[22] proposed a simple model for the axial mass transfer in gas-segmented straight cylindrical channel based on the assumptions that there is a perfect mixing in each liquid slug and mass transfer from the recirculating bulk liquid region to the film region can be characterized by an adjustable mass transfer coefficient. Bercic and Pintar[3] developed a computational model for the effects of gas bubbles and liquid slug length on the backmixing in the gas-segmented flow and found that the mass transfer mainly depends on the slug length and velocity. Thulasidas *et al.*[21] improved two-region model of Pedersen

[a)]Electronic mail: mmuradoglu@ku.edu.tr. Telephone: +90 (212) 338 14 73. Fax: +90 (212) 338 15 48.

and Horvath[22] by solving one-dimensional diffusion equation in the radial direction to account for the mass transfer by molecular diffusion. Salman *et al.*[23,24] developed a similar model based on the one-dimensional convection-diffusion equation. More recently they developed a computational fluid dynamics model for the axial dispersion and residence time distribution in a straight two-dimensional gas-segmented channel flow.[25] Muradoglu *et al.*[26] studied the axial dispersion in the gas-segmented flow using a finite-volume/front-tracking (FV/FT) method and examined the effects of the Peclet number, capillary number, and segment size in a straight two-dimensional channel. Kreutzer *et al.*[27] studied the axial dispersion in a straight rectangular microchannel and found that the liquid-filled menisci significantly increase the leakage and the axial dispersion is the least when the liquid flow rate is greater than the gas flow rate. Based on the work of Muradoglu and Stone,[14] Fries and von Rohr[13] and Dogan *et al.*[12] predicted that the channel curvature enhances the axial dispersion due to alternating film thickness in serpentine channels but they did not provide any detailed analysis.

In this paper, the effects of channel curvature on the axial dispersion are studied computationally using the finite-volume/front-tracking method in a two-dimensional setting to facilitate extensive numerical simulations. Note that microchannels usually have square or rectangular cross-section. Significant portion of leakage occurs through the corners of the rectangular channels at low Peclet numbers.[27] However the effects of large gutter in rectangular channel are expected to be small at high Peclet numbers. In addition, three dimensional microchannels of rectangular cross-section become quasi-two-dimensional when the aspect ratio of the channel cross-section is large, i.e., it is larger than eight.[28] Therefore the main conclusions of the present study are expected to be valid for the three dimensional rectangular channels at high Peclet numbers especially when the aspect ratio of the channel cross-section is large. Passive tracer particles are used to visualize and quantify the mass transfer. Molecular diffusion is modeled by a random walk of tracer particles in a similar fashion as done by Muradoglu *et al.*[26] The effects of the molecular diffusion are characterized by the Peclet number defined as $\mathrm{Pe}=V_c w/D$, where V_c, w, and D are the average liquid velocity in the channel, the channel width, and the molecular diffusivity, respectively. Extensive simulations are first performed to show and quantify the effects of the channel curvature on the axial dispersion in the absence of molecular mixing, i.e., as $\mathrm{Pe}\to\infty$. Based on the alternating film thickness in the serpentine channel,[14] a simple analytical model is developed and compared with the numerical results. Reasonable agreement is found between the analytical model and the computational simulations. The computations are then performed to show the effects of the molecular diffusion. It is found that the axial dispersion is always larger in a serpentine channel than that in the corresponding straight channel but the effects of channel curvature are more pronounced at high Peclet numbers, i.e., $\mathrm{Pe}>10^4$. It is also found that the difference between the straight and curved channels decreases continuously as the Peclet number decreases and becomes negligible at low Peclet numbers, i.e., $\mathrm{Pe}<10^3$.

The rest of the paper is organized as follows. The mathematical formulation and numerical method are briefly summarized in the next section. The physical problem is described in Sec. III. The results are presented and discussed in Sec. IV where the model is also described. Finally conclusions are drawn in Sec. V.

II. FORMULATION AND NUMERICAL METHOD

The governing equations are described here in the framework of the finite-volume/front-tracking method.[29–31] In the Cartesian coordinates, the two-dimensional incompressible continuity and Navier–Stokes equations can be written in conservation form as

$$\frac{\partial \mathbf{q}}{\partial t}+\frac{\partial \mathbf{f}}{\partial x}+\frac{\partial \mathbf{g}}{\partial y}=\frac{\partial \mathbf{f}_v}{\partial x}+\frac{\partial \mathbf{g}_v}{\partial y}+\mathbf{f}_b, \tag{1}$$

where

$$\mathbf{q}=\begin{Bmatrix}0\\ \rho u\\ \rho v\end{Bmatrix},\quad \mathbf{f}=\begin{Bmatrix}u\\ \rho u^2+p\\ \rho uv\end{Bmatrix},\quad \mathbf{g}=\begin{Bmatrix}v\\ \rho uv\\ \rho v^2+p\end{Bmatrix}, \tag{2}$$

and

$$\mathbf{f}_v=\begin{Bmatrix}0\\ \tau_{xx}\\ \tau_{xy}\end{Bmatrix},\quad \mathbf{g}_v=\begin{Bmatrix}0\\ \tau_{xy}\\ \tau_{yy}\end{Bmatrix}. \tag{3}$$

In Eqs. (1)–(3), x and y are the Cartesian coordinates and t is the time; ρ, μ, and p are the fluid density, the dynamic viscosity, and pressure, respectively, and u and v are the velocity components in x and y coordinate directions, respectively. The first row in Eq. (1) simply states that the velocity field is solenoidal while the last two rows represent the momentum conservation equations in the x and y directions, respectively. The viscous stresses appearing in the viscous flux vectors are given by

$$\tau_{xx}=2\mu\frac{\partial u}{\partial x},\quad \tau_{yy}=2\mu\frac{\partial v}{\partial y},\quad \tau_{xy}=\mu\left(\frac{\partial u}{\partial y}+\frac{\partial v}{\partial x}\right). \tag{4}$$

The last term in Eq. (1) represents the body forces resulting from surface tension and is given by

$$\mathbf{f}_b=\int_S \sigma\kappa\mathbf{n}\delta(\mathbf{x}-\mathbf{x}^f)ds, \tag{5}$$

where δ, $\mathbf{x}^f$, σ, κ, $\mathbf{n}$, S, and ds denote, respectively, the Dirac delta function, the location of the interface, the surface tension coefficient, twice the mean curvature, the outward unit normal vector on the interface, the surface area of the interface, and the surface area element of the interface.

In Eq. (1), it is assumed that the material properties of a fluid particle remain constant, i.e.,

$$\frac{D\rho}{Dt}=0;\quad \frac{D\mu}{Dt}=0, \tag{6}$$

where the substantial derivative is defined as

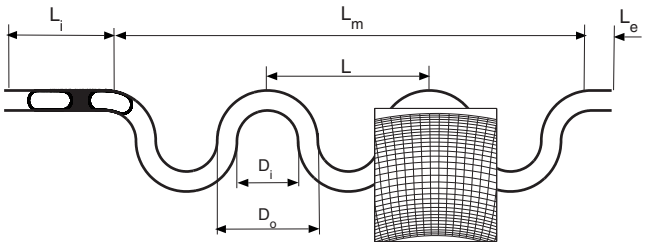

FIG. 1. The sketch of the channel used in the computations. The inset shows a portion of coarse grid containing 600×32 grid cells.

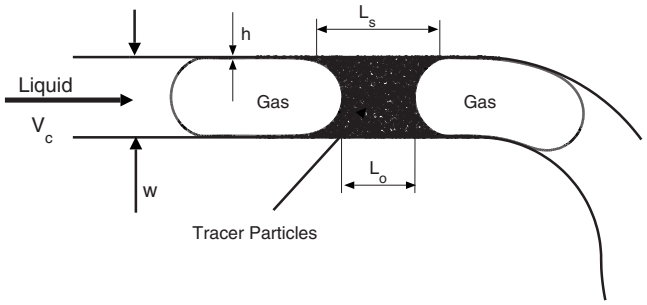

FIG. 2. A schematic illustration of the inlet portion of a two-dimensional channel containing two bubbles and one liquid segment. A large number of tracer particles is distributed at random in the liquid segment after gas bubbles reach their steady shapes.

$$\frac{D}{Dt} = \frac{\partial}{\partial t} + \mathbf{u} \cdot \nabla.$$

The governing equations [Eq. (1)] are solved by the finite-volume/front-tracking method developed by Muradoglu and Kayaalp.[31] The method combines a finite-volume solver with the front-tracking method developed by Unverdi and Tryggvason.[29] The continuity and momentum equations are solved on a curvilinear grid using a finite-volume method. The spatial derivatives are approximated by a finite-volume method that is equivalent to second-order finite differences on a regular mesh. A dual (or pseudo) time-stepping method is employed to achieve time accuracy and an alternating direction implicit (ADI) method is used to perform integration in pseudotime. Fourth-order numerical dissipation terms are added to the discrete version of the flow equations to prevent the odd-even decoupling. Preconditioning, local time-stepping, and multigrid methods are used to accelerate the convergence rate of the ADI method in the pseudotime. Details of the FV method can be found in Refs. 31 and 32.

The interface boundary between the bubble phase and the ambient fluid are represented by connected Lagrangian marker points moving with the local flow velocity interpolated from the neighboring curvilinear grid points. The communication between the curvilinear grid and the interface marker points is maintained efficiently using an auxiliary regular Cartesian grid cast on the curvilinear grid.[31] An indicator function is defined such that it is unity inside the droplet and zero outside. The indicator function is computed at each time step based on the locations of the interface marker points as described by Tryggvason *et al.*[30] and Muradoglu and Kayaalp.[31] Once the indicator function distribution is determined, the density and viscosity are set as a function of the indicator function. The interface marker points are also used to compute the surface tension forces at the interface which are then distributed on the neighboring curvilinear grid cells in a conservative manner and added to the discrete momentum equations as source terms. For the details of the FV/FT method, see Muradoglu and Kayaalp[31] and Muradoglu and Gokaltun.[33]

Passive tracer particles are used to visualize and quantify the axial dispersion in a similar way as done by Muradoglu *et al.*[26] The molecular mixing is modeled by random walk of tracer particles. In a Lagrangian frame, the location of mth particle $\mathbf{X}_m$ evolves by

$$d\mathbf{X}_m = \mathbf{U}_m dt + \sqrt{2D} d\mathbf{W}, \tag{7}$$

where $\mathbf{U}_m$ is the velocity interpolated from the Eulerian curvilinear grid onto the location of the tracer particle, dt is the time increment, D is molecular diffusivity of the tracer, and $d\mathbf{W}$ is a vector valued Wiener process[34] with the well-known properties of $\langle d\mathbf{W} \rangle = 0$ and $\langle dW_i dW_j \rangle = \delta_{ij} dt$, where $\langle \cdots \rangle$ denotes the mean and δ_{ij} is the Kronecker delta. Equation (7) is solved numerically using a predictor-corrector method together with the flow equations as described by Muradoglu *et al.*[26] The tracer particles crossing the channel wall or the bubble interfaces are reflected back into liquid region assuming a perfect collision. Note that the indicator function is utilized to reflect the particles crossing the bubble interface as described by Muradoglu *et al.*[26] while reflection is achieved using the geometric information for the particles crossing the channel walls.

III. PROBLEM STATEMENT

The effects of the channel curvature on the axial dispersion in gas-segmented flow in a serpentine channel are studied in a two-dimensional setting to facilitate extensive computational simulations. The model channel consists of a straight entrance, a curved mixer of three periods, and a straight exit section as sketched in Fig. 1. The curved section of the mixer consists of concentric circular arcs and the inner circle of a half period connects tangentially with the outer circle of the next half period. The diameters of the inner and outer arcs are D_i and D_o, respectively. The channel width is then given by $w = (D_o - D_i)/2$. Finally we complete the specification of the geometry by fixing L_i, the length of the inlet portion of the channel, L_e, the length of the exit portion of the channel, and L_m, the length of the mixing portion of the channel as sketched in Fig. 1. The inlet portion of the channel that contains the gas bubbles and the initial distribution of the tracer particles are shown in Fig. 2. The flow rate is specified at the inlet assuming a fully developed velocity profile with an average velocity of V_c. The flow is initialized as follows: a steady single-phase flow is computed first using the liquid properties and is then used as initial flow field. The bubbles are instantaneously placed in the channel close to the inlet with an approximate shape consisting of a straight middle and semicircular front and back sections. Passive

tracer particles are initially distributed uniformly at random in the channel outside of the bubbles when the bubbles take their steady shapes in the inlet section of the channel as shown in Fig. 2. The particles are moved with the local flow velocity interpolated from the neighboring computational grid points using the same advection scheme as used for moving the interface marker points.

The properties of gas bubble and liquid are denoted by subscripts i and o, respectively. The governing nondimensional parameters are defined as the channel Reynolds number $\mathrm{Re}=\rho_o V_c w/\mu_o$, the capillary number $\mathrm{Ca}=\mu_o V_c/\sigma$, the Peclet number $\mathrm{Pe}=V_c w/D$, the viscosity ratio $\lambda=\mu_i/\mu_o$, the density ratio $r=\rho_i/\rho_o$, the normalized distance between the gas bubbles in the inlet section $\eta=L_o/w$, the normalized curvature of the inner channel wall $\beta=2w/D_i$, and the normalized equivalent bubble diameter $\Lambda=d_b/w$ where d_b is the equivalent bubble diameter. The nondimensional time is defied as $t^*=tV_c/w$. Note that all the computations presented in this paper are performed at $\mathrm{Re}=0.64$, $\lambda=0.1$, $r=0.1$, $\Lambda=1.5$, and $\beta=0.667$. It is emphasized here that these viscosity and density ratios are much larger than the typical values encountered in microfluidic applications. For instance, $\lambda\sim 0.01$ and $r\sim 0.001$ for ethanol/air or water/air systems. However, the effects of viscosity and density ratios are expected to be small when $\lambda\leq 0.1$ and $r\leq 0.1$ for the kind of problems studied here.[14,26]

The averaged tracer concentration in the liquid slug is defined as

$$\langle C\rangle = \frac{N}{A_s}, \tag{8}$$

where N is the total number of particles in the liquid slug between the centroids of the bubbles and A_s is the area of the slug. The slug area is assumed to remain constant throughout the simulation so that the normalized average tracer concentration is simply computed as

$$\frac{\langle C\rangle}{\langle C\rangle_i} = \frac{N}{N_i},$$

where N_i is the initial number of tracer particles in the slug.

IV. RESULTS AND DISCUSSION

Extensive computational simulations are performed to examine the effects of the channel curvature on the axial dispersion. A portion of a typical (coarse) curvilinear grid containing 600×32 grid cells is shown in the inset of Fig. 1 to show the overall grid structure. The computations are performed on a finer version of this grid that contains 2400×128 grid cells. As can be seen in Fig. 1, the grid is stretched near the channel walls in order to resolve the thin liquid films between the bubbles and the channel. The grid convergence of the present numerical method has been extensively examined and this grid resolution has been shown to be sufficient to achieve grid independent solutions for this kind of problems as long as $\mathrm{Ca}\geq 0.005$.[12,14,26,35] Therefore such an extensive grid convergence study is not repeated here. Note that the capillary number is often smaller than 0.005 in microfluidic applications[11,27] but the simulations are limited to this value in the present study mainly due to the excessive computational cost required to resolve thin liquid film region that is of critical importance for the axial dispersion.

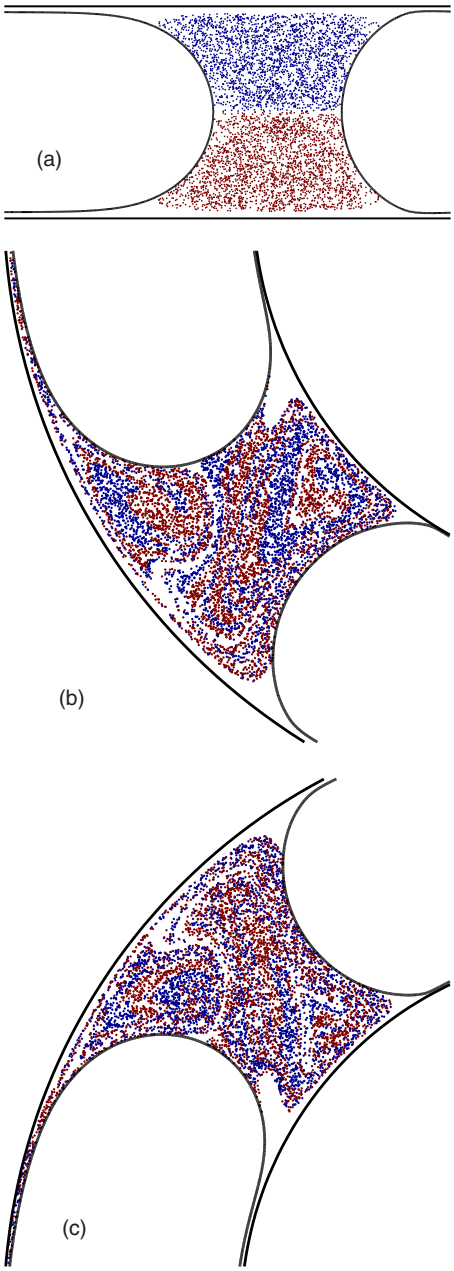

FIG. 3. (Color online) Scatter plots of the tracer particles showing the enhancement of the axial dispersion due to the channel curvature in the absence of the molecular diffusion. Different colors are used for the particles initially located in the lower and upper portions of the liquid segment to show the mixing patterns as well as the axial dispersion. There is no axial dispersion in the case of the straight channel (a) but there is significant axial dispersion for the case of the curved channel (b) in the convex and (c) the concave segments ($\mathrm{Ca}=0.01$, $\mathrm{Re}=0.64$, $\lambda=0.1$, $r=0.1$, $\Lambda=1.5$, and $\beta=0.667$).

First, the molecular diffusion is switched off in order to examine the sole effects of the channel curvature on the axial dispersion. For this purpose, the scatter plots of the tracer particles are plotted in Fig. 3 for the straight and curved channel cases. As can be seen in this figure, a lubricating thin

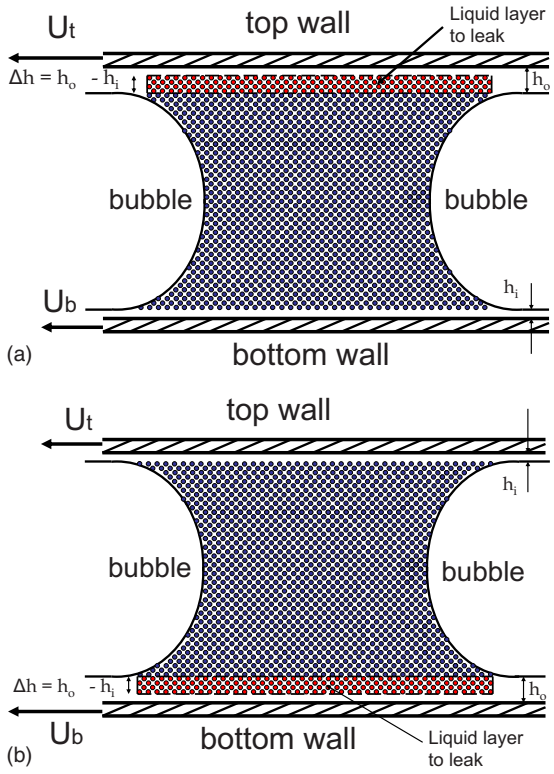

FIG. 4. (Color online) Schematic illustration of the model for the leakage through liquid films (a) at the top and (b) at the bottom of the channel.

liquid film forms on the wall of the straight channel and persists as the bubbles pass leading to no axial dispersion. In the case of serpentine channel, however, this lubricating liquid film is broken periodically resulting in significant axial dispersion as seen in Figs. 3(b) and 3(c). It is also seen in this figure that there is still a thin lubricating liquid film even in the case of the serpentine channel and leakage occurs due to alternating film thickness. It is seen visually from these scatter plots that the liquid layer with an approximate width of $\Delta h = h_o - h_i$ leaks in every half period where h_i and h_o are the film thickness on the inner and outer channel walls, respectively. The leakage occurs through the liquid film on the outer wall, once on the one side and then on the other side of the channel as shown in Fig. 3. As recently discussed by Dogan *et al.*,[12] in the coordinate system moving with the centroid of the liquid slug, the velocities at the inner and outer wall can be approximated by $U_t = 2(1+\beta)V_b/(2+\beta)$ and $U_b = 2V_b/(2+\beta)$, respectively, and the flow in the liquid slug resembles a double-lid-driven cavity flow with liquid leakage through the edges at small capillary numbers. Using this analogy, each half period of the curved channel can be mapped into a straight channel segment with alternating liquid film thickness and wall velocity as sketched in Fig. 4. In the first half period, the leakage occurs through the liquid film on the upper wall and then through the liquid film on the lower wall in a periodic fashion. The amount of tracer that leaks in each half period $\tau_{h\text{period}}$ can be approximated as $\Delta h L_s \langle C \rangle$ where L_s is the length of the liquid layer (Fig. 2). Assuming that the liquid slug is well mixed due to the chaotic advection in each half period, the average concentration in the liquid slug decays according to

$$\frac{\langle C \rangle}{\langle C \rangle_i} = e^{-\alpha t^*}, \tag{9}$$

where $\langle C \rangle_i$ is the initial average concentration and

$$\alpha = \frac{\Delta A_h}{A_s} \frac{1}{\tau_{h\ \text{period}}} \frac{w}{V_c}. \tag{10}$$

In Eq. (10), A_s is the area of the liquid slug, ΔA_h is the area of liquid layer that leaks through the outer film in the half period. The area of the liquid layer is computed as $\Delta A_h = \Delta h L_s$ and the half time period is approximated as $\tau_{h\ \text{period}} = \pi(R_i + w/2)/V_b$, where V_b is the average bubble velocity. Based on the analysis due to Muradoglu and Stone,[14] the film thicknesses on the inner and outer walls of the curved channel can be computed as

$$h_i = 1.3375 R_{\text{eff}_i}\, \text{Ca}_{\text{eff}_i}^{2/3}, \quad h_o = 1.3375 R_{\text{eff}_o}\, \text{Ca}_{\text{eff}_o}^{2/3}, \tag{11}$$

where

$$R_{\text{eff}_i} = \frac{1}{2+\beta}; \quad R_{\text{eff}_o} = \frac{1+\beta}{2+\beta};$$
$$\text{Ca}_{\text{eff}_i} = \frac{2+2\beta}{2+\beta}\text{Ca}; \quad \text{Ca}_{\text{eff}_o} = \frac{2}{2+\beta}\text{Ca}. \tag{12}$$

In Eq. (12), $\beta = 2w/D_i$ is the nondimensional channel curvature and $\text{Ca} = \mu_o V_c/\sigma$ is the capillary number. Equation (11) is valid only for small capillary numbers, i.e., $\text{Ca} \ll 1$. For larger capillary numbers, this equation can be modified as

$$\frac{h_{i,o}}{R_{\text{eff}_{i,o}}} = \frac{1.34\ \text{Ca}_{\text{eff}_{i,o}}^{2/3}}{1 + 1.34 \times 2.5\ \text{Ca}_{\text{eff}_{i,o}}}, \tag{13}$$

which is based on the correlation suggested by Aussilous and Quere[36] and has been also shown to agree very well with the numerical simulations for a wide range of capillary numbers in curved channels.[14] Note that microchannels usually have square or rectangular cross-section and a significant portion of leakage occurs through the corners of the rectangular channels at low Peclet numbers.[27] However the effects of a large gutter in rectangular channel are expected to be small at high Peclet numbers since the leakage is solely caused by the alterations in the liquid film thickness in the limit of vanishing molecular diffusion. In addition, three dimensional microchannels of rectangular cross-section become quasi-two-dimensional when the aspect ratio of the channel cross-section is large, i.e., it is larger than eight.[28] Therefore the main conclusions of the present study are expected to be valid for the three dimensional rectangular channels at high Peclet numbers especially when the aspect ratio of the channel cross-section is large.

The theory developed above is tested against the numerical simulations. For this purpose, the computations are performed for two different capillary numbers, i.e., Ca=0.01 and Ca=0.005. The relative distance between bubbles is about $L_o/w = 0.62$ and $L_o/w = 0.64$ for Ca=0.01 and Ca =0.005, respectively. The evolution of average tracer concentration is plotted in Fig. 5 where Eq. (9) is shown as dashed curves. Since the theory is valid only after the initial

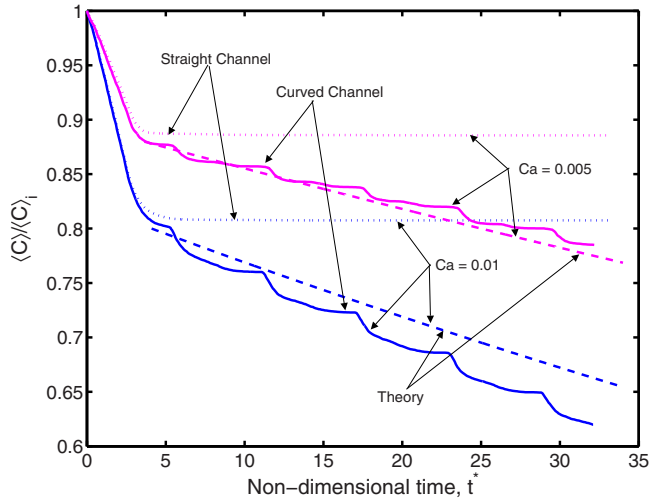

FIG. 5. (Color online) Effects of the channel curvature on the axial dispersion. The relative distance between bubbles are $L_o/w=0.62$ and $L_o/w=0.64$ for Ca=0.01 and Ca=0.005, respectively. The computational results for the serpentine channel (solid lines) are compared with the theoretical results (dashed lines). The corresponding results for the straight channels are also shown by dotted lines (Re=0.64, $\lambda=0.1$, $r=0.1$, $\Lambda=1.5$, and $\beta=0.667$).

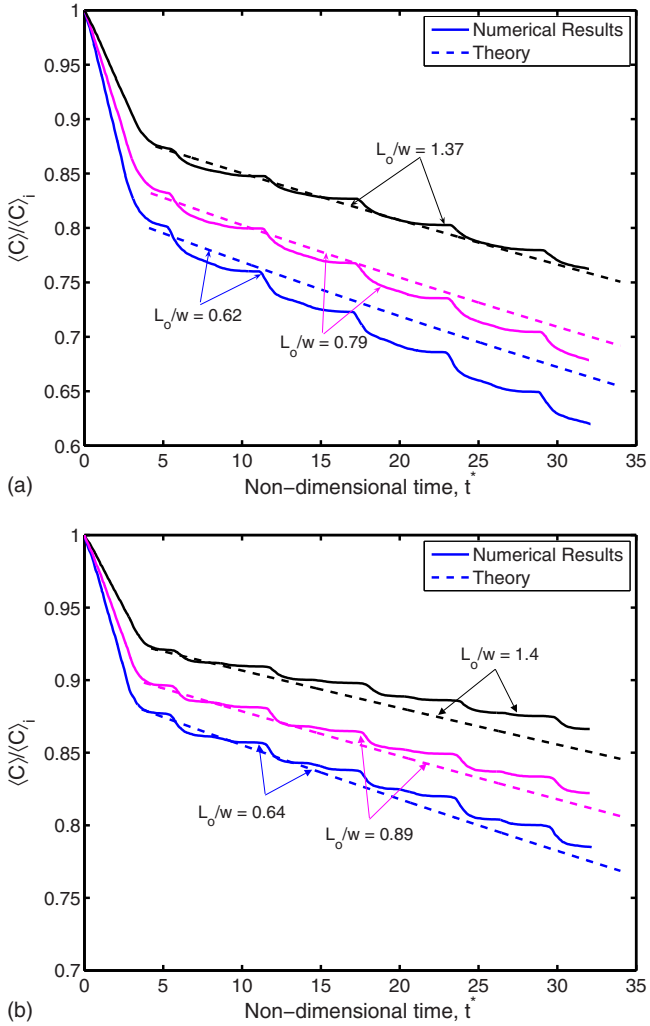

FIG. 6. (Color online) Effects of the relative distance between bubbles on the axial dispersion for (a) Ca=0.01 and (b) Ca=0.005. The theoretical predictions are shown by dashes lines (Re=0.64, $\lambda=0.1$, $r=0.1$, $\Lambda=1.5$, and $\beta=0.667$).

period in which the concentration is reduced just because the tracer particles originally in the film region are convected downstream (relative to the coordinate system fixed to a bubble), the time is started after this initial period in all the theoretical results presented here. As can be seen in this figure, there is significant axial dispersion in curved channels and the leakage increases with increasing capillary number. On the other hand, there is no axial dispersion in the straight channel case except for the initial period as also shown by Muradoglu *et al.*[26] The theoretical results are in a reasonably good agreement with the computational simulations for both capillary numbers. The discrepancy between the theoretical and computational results can be partly attributed to the uncertainties in computing slug area and slug length used in Eq. (10). It is interesting to observe that the decay rate is overpredicted for Ca=0.01 while it is underpredicted for Ca=0.005, and the theoretical prediction is in a better agreement with the computational result for Ca=0.005. Note that the bumpy feature observed in the evolution of the average concentration in serpentine channel is mainly caused by the rapid change in liquid film thickness as a result of change in the channel curvature when the bubbles move from one half period to the next. Consequently, a large amount of tracer particles is convected rapidly through the enlarged liquid film at the beginning of each half period.

Next, the effects of the relative distance between bubbles are investigated. For this purpose, the molecular diffusion is again switched off and the computations are performed for three values of relative distance between bubbles at Ca=0.01 and Ca=0.005. Note that the uncertainties in computing slug area and slug length decrease as the distance between the bubbles increases. But, at the same time, the quality of mixing deteriorates as the slug length increases as discussed recently by Dogan *et al.*[12] The computational results are plotted in Figs. 6(a) and 6(b) for $L_o/w=0.62$, 0.79, and 1.37 at Ca=0.01 and for $L_o/w=0.64$, 0.89, and 1.4 at Ca=0.005, respectively. The computational results are compared with the theory for all the cases. The concentration decay rate is consistently overpredicted for Ca=0.01 while it is underpredicted for Ca=0.005 for all values of L_o/w. Figure 6 also shows that the decay rate decreases with increasing L_o/w just because the slug size gets larger and thus it takes a longer time for the tracer particles to leak through the liquid film.

Finally the effects of the molecular diffusion are investigated. For this purpose, the Peclet number is varied in the range between Pe=100 and $\mathrm{Pe}\to\infty$ and computations are repeated for Ca=0.01 and Ca=0.005 in both the straight and serpentine channel cases. The molecular diffusion is expected to increase the axial dispersion due to the enhanced mass transfer from the slug to the wall region as well as improved mixing within the liquid slug. The effects of the molecular diffusion on the axial dispersion have been recently studied extensively in straight channel case by Muradoglu *et al.*[26] Therefore the emphasis is placed here on the effects of the channel curvature in the presence of mo-

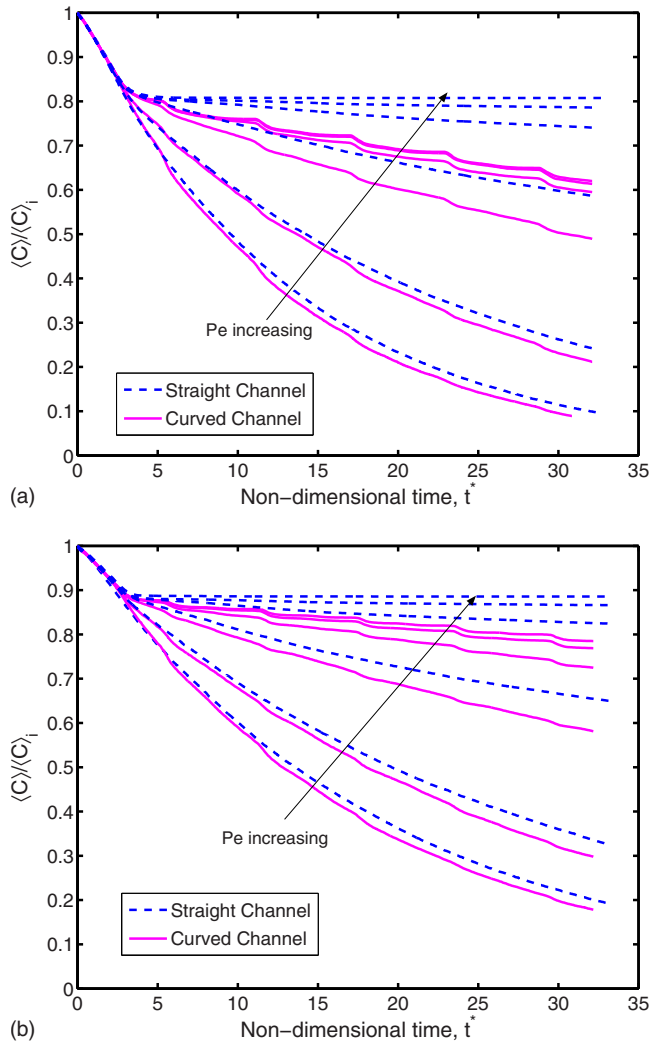

FIG. 7. (Color online) Effects of molecular diffusion. (a) Ca=0.01 and $L_o/w=0.62$. (b) Ca=0.005 and $L_o/w=0.64$ (Re=0.64, $\lambda=0.1$, $r=0.1$, $\Lambda=1.5$, and $\beta=0.667$).

lecular diffusion. The time evolution of the tracer concentration is plotted in Figs. 7(a) and 7(b) for Ca=0.01 and Ca=0.005, respectively. As can be seen in these figures, the axial dispersion increases monotonically with decreasing Peclet number both for the straight and curved channel cases. The axial dispersion is always larger in the serpentine channel than that in the straight channel. However, the effects of channel curvature reduce as Peclet number decreases and becomes negligible at very low Peclet numbers since the axial dispersion is mainly controlled by the convection through the liquid film in the low Peclet number limit as $\mathrm{Pe}\rightarrow 0$. On the other hand, the effects of channel curvature increase rapidly at high Peclet numbers, i.e., $\mathrm{Pe}>10^4$, and the axial dispersion is solely caused by alternating channel curvature as $\mathrm{Pe}\rightarrow\infty$.

V. CONCLUSIONS

Effects of channel curvature on the axial dispersion in gas-segmented liquid flow are studied computationally using a finite-volume/front-tracking method. A large number of passive tracer particles are used to visualize and quantify the axial dispersion. Molecular diffusion is modeled by the random walk of the tracer particles. The particles crossing the liquid-solid and liquid-gas interfaces are reflected back into the liquid region using a perfect elastic collision model. Geometric information is used to reflect the particles crossing the solid wall while the indicator function is utilized for the particles crossing the liquid-gas interfaces as described by Muradoglu *et al.*[26] Computations are performed in a two-dimensional setting to facilitate extensive numerical simulations.

The molecular diffusion is first switched off in order to demonstrate the axial dispersion solely due to the alternating film thickness in a serpentine channel. It is found that the lubricating thin liquid layer that persists on the wall of a straight channel is periodically broken in the curved channel case leading to significant axial dispersion. It is confirmed that there is no axial dispersion in a straight channel in the absence of molecular diffusion after the initial period in which the particles originally in the liquid film region are simply convected downstream. A model is proposed for the enhancement of axial dispersion in serpentine channel based on the difference between the liquid film thickness on the inner and outer channel walls. The model assumes a perfect mixing within the liquid slug in each half period, a condition that is usually well satisfied in applications due to chaotic stirring. The model predicts that concentration of the tracer within the liquid slug decays exponentially in time and the decay rate is proportional to the difference between the liquid film thickness in successive half periods. It is found that the model predicts the decay rate of the tracer concentration reasonably well compared to the computational results. The axial dispersion strongly depends on the capillary number and increases as capillary number increases. The theoretical prediction is found to be in a better agreement with the computational results for smaller capillary numbers. The effects of the liquid slug length or equivalently the distance between the gas bubbles are also investigated. It is found that the tracer concentration decays faster as the slug length decreases. This is mainly due to the fact that it takes longer time for tracer within a large liquid slug to leak through the film and also partly due to the enhanced mixing in small liquid slugs.

Then the combined effects of channel curvature and molecular diffusion are studied. Computations are performed both for the straight and serpentine channel cases for a range of Peclet numbers between Pe=100 and $\mathrm{Pe}\rightarrow\infty$. It is found that the effects of the channel curvature are more pronounced at high Peclet numbers, i.e., $\mathrm{Pe}>10^4$. The axial dispersion is primarily controlled by the convection through the liquid films and thus the effects of the channel curvature are marginal at low Peclet numbers, i.e., $P<100$. On the other hand, the axial dispersion is mainly controlled by the quality of mixing due to chaotic advection and alternating film thickness in the high Peclet number limit, i.e., $\mathrm{Pe}>10^6$. In between, there is a transition regime where both the channel curvature and molecular mixing are important.

ACKNOWLEDGMENTS

The author thanks Professor Howard A. Stone for helpful conversations. This work has been supported by the Scientific and Technical Research Council of Turkey (TUBITAK) with Grant No. 108M238 and Turkish Academy of Sciences (TUBA-GEBIP).

[1] G. I. Taylor, "Deposition of viscous fluid on the wall of a tube," J. Fluid Mech. **10**, 161 (1960).
[2] F. P. Bretherton, "The motion of long bubbles in tubes," J. Fluid Mech. **10**, 166 (1961).
[3] G. Bercic and A. Pintar, "The role of gas bubbles and liquid slug length on mass transport in the Taylor flow through capillaries," Chem. Eng. Sci. **52**, 3709 (1997).
[4] S. Irandoust and B. Andersson, "Mass-transfer and liquid-phase reaction in a segmented two-phase flow monolithic catalyst reactor," Chem. Eng. Sci. **43**, 1983 (1988).
[5] M. T. Kreutzer, F. Kapteijn, J. A. Moulijn, and J. J. Heiszwolf, "Multiphase monolith reactors: Chemical reaction engineering of segmented flow in microchannels," Chem. Eng. Sci. **60**, 5895 (2005).
[6] R. H. Patrick, T. Klindera, L. L. Crynes, R. L. Cerro, and M. A. Abraham, "Residence time distribution in 3-phase monolith reactor," AIChE J. **41**, 649 (1995).
[7] B. K. Paul and S. P. Moulik, "Microemulsions: An overview," J. Dispersion Sci. Technol. **18**, 301 (1997).
[8] L. T. Skeggs, "An automatic method for colorimetric analysis," Am. J. Clin. Pathol. **28**, 311 (1957).
[9] L. R. Snyder and H. J. Adler, "Dispersion in segmented flow through glass tubing in continuous-flow analysis—Ideal model," Anal. Chem. **48**, 1017 (1976).
[10] L. R. Snyder and H. J. Adler, "Dispersion in segmented flow through glass tubing in continuous-flow analysis—Nonideal model," Anal. Chem. **48**, 1022 (1976).
[11] A. Günther, S. A. Khan, M. Thalmann, F. Trachsel, and K. F. Jensen, "Transport and reaction in microscale segmented gas-liquid flow," Lab Chip **4**, 278 (2004).
[12] H. Dogan, S. Nas, and M. Muradoglu, "Mixing of miscible liquids in gas-segmented serpentine channels," Int. J. Multiphase Flow **35**, 1149 (2009).
[13] D. M. Fries and P. R. von Rohr, "Liquid mixing in gas-liquid two-phase flow by meandering microchanels," Chem. Eng. Sci. **64**, 1326 (2009).
[14] M. Muradoglu and H. A. Stone, "Motion of large bubbles in curved channels," J. Fluid Mech. **570**, 455 (2007).
[15] A. Günther and K. F. Jensen, "Multiphase microfluidics: From flow characteristics to chemical and material synthesis," Lab Chip **6**, 1487 (2006).
[16] N. de Mas, A. Günther, M. A. Schmidt, and K. F. Jensen, "Increasing productivity of microreactors for fast gas-liquid reactions: The case of direct fluorination of toluene," Ind. Eng. Chem. Res. **48**, 1428 (2009).
[17] B. K. H. Yen, A. Günther, M. A. Schmidt, K. F. Jensen, and M. G. Bawendi, "A microfabricated gas-liquid segmented flow reactor for high-temperature synthesis: The case of CdSe quantum dots," Angew. Chem., Int. Ed. **44**, 5447 (2005).
[18] F. Trachsel, A. Günther, S. Khan, and K. F. Jensen, "Measurement of residence time distribution in microfluidic systems," Chem. Eng. Sci. **60**, 5729 (2005).
[19] M. T. Kreutzer, J. J. W. Bakker, F. Kapteijn, J. A. Moulijn, and P. J. T. Verheijen, "Scaling-up multiphase monolith reactors: Linking residence time distribution and feed maldistribution," Ind. Eng. Chem. Res. **44**, 4898 (2005).
[20] T. C. Thulasidas, M. A. Abraham, and R. L. Cerro, "Dispersion during bubble-train flow in capillaries," Chem. Eng. Sci. **54**, 61 (1999).
[21] T. C. Thulasidas, M. A. Abraham, and R. L. Cerro, "Flow patterns in liquid slugs during bubble-train flow inside capillaries," Chem. Eng. Sci. **52**, 2947 (1997).
[22] H. Pedersen and C. Horvath, "Axial dispersion in a segmented gas-liquid flow," Ind. Eng. Chem. Fundam. **20**, 181 (1981).
[23] W. Salman, A. Gavriilidis, and P. Angeli, "A model for predicting axial mixing during gas-liquid Taylor flow in microchannels at low Bodenstein numbers," Chem. Eng. J. **101**, 391 (2004).
[24] W. Salman, A. Gavriilidis, and P. Angeli, "Sample pulse broadening in Taylor flow microchannels for screening applications," Chem. Eng. Technol. **28**, 509 (2005).
[25] W. Salman, A. Gavriilidis, and P. Angeli, "Axial mass transfer in Taylor flow through circular microchannels," AIChE J. **53**, 1413 (2007).
[26] M. Muradoglu, A. Günther, and H. A. Stone, "A computational study of axial dispersion in segmented gas-liquid flow," Phys. Fluids **19**, 072109 (2007).
[27] M. T. Kreutzer, A. Günther, and K. J. Jensen, "Sample dispersion for segmented flow in microchannels with rectangular cross-section," Anal. Chem. **80**, 1558 (2008).
[28] A. De Lózar, A. Juel, and A. L. Hazel, "The steady propagation of an air finger into a rectangular tube," J. Fluid Mech. **614**, 173 (2008).
[29] S. O. Unverdi and G. Tryggvason, "A front-tracking method for viscous, incompressible flows," J. Comput. Phys. **100**, 25 (1992).
[30] G. Tryggvason, B. Bunner, A. Esmaeeli, D. Juric, N. Al-Rawahi, W. Tauber, J. Han, S. Nas, and Y.-J. Jan, "A front-tracking method for the computations of multiphase flow," J. Comput. Phys. **169**, 708 (2001).
[31] M. Muradoglu and A. D. Kayaalp, "An auxiliary grid method for computations of multiphase flows in complex geometries," J. Comput. Phys. **214**, 858 (2006).
[32] D. A. Caughey, "Implicit multigrid computation of unsteady flows past cylinders of square cross-section," Comput. Fluids **30**, 939 (2001).
[33] M. Muradoglu and S. Gokaltun, "Implicit multigrid computations of buoyant drops through sinusoidal constrictions," Trans. ASME, J. Appl. Mech. **71**, 857 (2004).
[34] S. B. Pope, *Turbulent Flows* (Cambridge University Press, Cambridge, 2000).
[35] M. Muradoglu and H. A. Stone, "Mixing in a drop moving through a serpentine channel: A computational study," Phys. Fluids **17**, 073305 (2005).
[36] P. Aussillous and D. Quere, "Quick deposition of a fluid on the wall of a tube," Phys. Fluids **12**, 2367 (2000).